View metadata, citation and similar papers at core.ac.uk

brought to you by CORE

provided by Boston University Institutional Repository (OpenBU)

Boston University

OpenBU **http://open.bu.edu**

BU Open Access Articles BU Open Access Articles

2006

Secondary structure effects on DNA hybridization kinetics: a solution versus surface comparison

This work was made openly accessible by BU Faculty. Please share how this access benefits you. Your story matters.

Version	
Citation (published version):	Yang Gao, Lauren K Wolf, Rosina M Georgiadis. 2006. "Secondary structure effects on DNA hybridization kinetics: a solution versus surface comparison.." Nucleic Acids Res, v. 34, issue 11, pp. 3370 - 3377.

https://hdl.handle.net/2144/29263

Boston University

Boston University Libraries
OpenBU

3370–3377 *Nucleic Acids Research, 2006, Vol. 34, No. 11*
doi:10.1093/nar/gkl422

Secondary structure effects on DNA hybridization kinetics: a solution versus surface comparison

Yang Gao, Lauren K. Wolf and Rosina M. Georgiadis*

Department of Chemistry, Metcalf Center for Science and Engineering, Boston University, 590 Commonwealth Avenue, Boston, MA 02215, USA

Received February 21, 2006; Revised May 5, 2006; Accepted May 27, 2006

ABSTRACT

The hybridization kinetics for a series of designed 25mer probe–target pairs having varying degrees of secondary structure have been measured by UV absorbance and surface plasmon resonance (SPR) spectroscopy in solution and on the surface, respectively. Kinetic rate constants derived from the resultant data decrease with increasing probe and target secondary structure similarly in both solution and surface environments. Specifically, addition of three intramolecular base pairs in the probe and target structure slow hybridization by a factor of two. For individual strands containing four or more intramolecular base pairs, hybridization cannot be described by a traditional two-state model in solution-phase nor on the surface. Surface hybridization rates are also 20- to 40-fold slower than solution-phase rates for identical sequences and conditions. These quantitative findings may have implications for the design of better biosensors, particularly those using probes with deliberate secondary structure.

INTRODUCTION

The process of hybridization, in which an oligonucleotide probe recognizes and binds to its complementary target, is the most vital component of DNA- and RNA-based biosensor technology. This technology, often used in conjunction with microarray surfaces, is being increasingly applied in gene sequencing, gene expression profiling and drug discovery. Factors such as ionic strength, sequence composition and temperature, which affect both surface (1,2) and solution-phase hybridization (3,4), have been characterized extensively. In fact, solution-phase hybridization studies have been so extensive that algorithms have been derived to quantitatively predict the thermodynamics of duplex formation for selected input sequences and conditions (5,6).

Similarly, algorithms have been designed to predict the folding or secondary structure present in single-stranded oligomers under various solution conditions (5,7,8). Not only does oligonucleotide secondary structure play an important role in biological recognition processes, but is also known to be an additional factor in duplex hybridization (9–11). Few studies, however, have attempted to quantitatively characterize the effects of sequence secondary structure on the kinetics and thermodynamics of hybridization in solution (12–15), or on the surface (16). With the advent of structured-probe biosensors, such as those incorporating hairpins, molecular beacons or aptamers, it becomes more important to understand these structural effects.

Generally, the intramolecular base pairs involved in secondary structure, stabilize single-strand conformation, creating a higher energy barrier to intermolecular hybridization. This, in turn, can slow hybridization kinetics. In practical biosensor applications, these effects are lessened by designing shorter single-stranded probe and target molecules or by increasing the 'incubation' temperature. Nevertheless, reducing strand length can also reduce biosensor detection sensitivity and increasing temperature, even to physiological values, does not always eliminate all effects (17). In addition, biosensors employing structured probes cannot be operated at high temperatures and maintain performance. As a result, there is a need for quantitative characterization of secondary structure effects on hybridization, particularly surface hybridization, using biosensor-relevant conditions.

To this end, we have systematically studied the effect of secondary structure on DNA–DNA hybridization kinetics both in solution and on the surface under identical conditions. We have used *in situ* UV absorbance and surface plasmon resonance (SPR) spectroscopy, respectively, to investigate duplex formation in a series of probe–target pairs containing varying well-defined degrees of secondary structure. Hybridization kinetic rates were suppressed as a function of individual strand secondary structure in a similar, clearly defined manner in solution and on the surface. Target hybridization on the surface was also 20–40 times slower than in solution for our system. In addition, probe and target pairs containing large amounts of secondary structure were shown to hybridize by a more complex mechanism than traditional two-state duplex formation. We have proposed, instead, a mechanism of fast nucleation and slow partial strand displacement.

*To whom correspondence should be addressed. Tel: +1 617 353 2500; Fax: +1 617 353 6466; Email: rgeorgia@bu.edu

© 2006 The Author(s).
This is an Open Access article distributed under the terms of the Creative Commons Attribution Non-Commercial License (http://creativecommons.org/licenses/by-nc/2.0/uk/) which permits unrestricted non-commerical use, distribution, and reproduction in any medium, provided the original work is properly cited.

Table 1. Oligonucleotide sequences and nomenclature

Probe	
P_0	5′-GTTGTCAAGATGCTACCGTTCAGAG-3′
P_3	5′-AGATCAGTGCGTCTGTACTAGCAGT-3′
P_4	5′-AGATCAGTGCGTCTGTACTAGCACA-3′
Target (complementary to the corresponding probe)	
T_0	5′-CTCTGAACGGTAGCATCTTGACAAC-3′
T_3	5′-ACTGCTAGTACAGACGCACTGATCT-3′
T_4	5′-TGTGCTAGTACAGACGCACTGATCT-3′

MATERIALS AND METHODS

Materials

All oligonucleotides were purchased from Integrated DNA Technologies (IDT). The sequences are listed in Table 1. All probe sequences employed in surface studies were modified at the 5′ terminus with a six-carbon linker and thiol group (HS-$(CH_2)_6$–). These sequences were received with a protecting group attached via disulfide bond. Before use, the protective disulfide bond was cleaved by incubating the oligonucleotides with 0.04 M DTT (Amersham Biosciences) in 0.17 M sodium phosphate buffer (pH = 8.0; Sigma) at room temperature for at least 16 h. The cleaved molecules were separated on a size-exclusion NAP-10 column (Amersham Biosciences). The concentration of thiolated DNA recovered from the column was determined by UV absorbance measurements at 260 nm (Varian Cary 100). All target and non-thiolated probe sequences employed in solution-phase studies were used as received.

Other chemicals employed in both solution-phase and surface studies were purchased from Sigma and used as received. These include mercaptohexanol (MCH), potassium dihydrogen phosphate (KH_2PO_4), sodium chloride (NaCl), ethylenediaminetetraacetic acid (EDTA), Trizma hydrochloride, Trizma Base and SDS. All buffers and immobilization solutions were prepared with 18 MΩ·cm distilled water.

Sequence selection

In order to systematically study the effects of secondary structure on DNA hybridization kinetics, we designed a series of short oligomers using mFold (5,7,8). The selected 25mer sequences, shown in Table 1, contain varying numbers of base pairs involved in intramolecular folding. The nucleobases participating in the secondary structure predicted by mFold are underlined for clarity. Although some of these sequences were predicted to have more than one possible conformation, only the lowest energy structures are considered (and underlined) here. Under the conditions employed in these studies, P_0 and T_0 have no secondary structure and are treated as random coils. Sequence pairs P_3T_3 and P_4T_4 contain 3 and 4 bp, respectively, in a hairpin-like stem on each strand. In addition to these complementary pairs, we also present kinetic data for the mismatched duplex, P_4T_3, which contains two terminal base pair mismatches (A·A and C·C).

Solution-phase studies

We qualitatively characterized the secondary structure of each single-stranded DNA (ssDNA) sequence designed for these studies by thermal melting. The UV absorbance of 2 μM ssDNA in 1, 0.5 and 0.1 M NaCl/TE buffer (TE: 10 mM Tris, pH 7.6 and 1 mM EDTA) was monitored at 260 nm while the temperature was ramped from 20 to 80°C at a rate of 0.5°C/min (Varian Cary 100 with a Peltier thermostatable multicell holder, temperature accuracy <±0.3°C). The duplex stability of each probe–target pair was also measured via thermal melting experiments in the same buffers; the temperature was ramped from 20 to 88°C at a slower rate of 0.25°C/min.

Kinetics of DNA hybridization was measured in three different ionic strength buffers: 1, 0.5 and 0.1 M NaCl/TE. Before hybridization, all target and probe molecules were separately annealed by rapidly heating each sequence to 80°C and slowly cooling to 20°C over an hour. Hybridization was then observed by monitoring the decrease in UV absorbance at 260 nm upon mixing equal molar concentrations of probe and target solutions. These solutions were mixed via hand pipetting or syringe injection into an empty 1 cm path-length semi-micro quartz cuvette. The cell was pre-equilibrated at 20°C and hybridization was monitored at this fixed temperature. The decrease in UV absorbance, caused by hypochromism that occurs during duplex formation, was monitored until there was no appreciable absorbance change over time. For hand mixing, the time required for pipetting the solutions into the cuvette and securing the instrument cover was ~3 s; no kinetic data were collected during this time and the initial absorbance (at $t = 0$) was calculated based on the concentration and molecular extinction coefficients of the single strands mixed. For syringe injection, kinetic data were collected continuously, but reasonable UV absorbance values were not obtained until the injected solution volume reached the instrumental beam height in the cuvette. Time zero ($t = 0$) was assigned to this 'reasonable' point during the filling of the cuvette, although the uncertainty in this selection can be as much as ±1 s. Nevertheless, we have found that varying the choice of time zero over this temporal range of uncertainty does not affect the kinetic rate constants obtained from fitting. In addition, the different mixing methods have no influence on the kinetic data obtained, as is demonstrated for P_0T_0 hybridization in 1 M NaCl/TE (Supplementary Figure S1).

Solution-phase kinetic analysis

The rate constants of solution-phase DNA hybridization were obtained by two different methods: linear and nonlinear second-order fits to the absorbance data. At time t, the concentration of ssDNA, C_t, is calculated using the following equation:

$$C_t = \frac{(A_t - A_\infty)}{(A_0 - A_\infty)} \cdot C_0, \quad \mathbf{1}$$

where A_t is the absorbance at time t, A_0 is the absorbance of the ssDNA at $t = 0$, A_∞ is the absorbance of the double-stranded DNA (dsDNA) at equilibrium and C_0 is the initial concentration of ssDNA. Hybridization of equal molar probe and target single strands can be described by second-order reaction kinetics:

$$\frac{1}{C_t} - \frac{1}{C_0} = k_{on} \cdot t, \quad \mathbf{2}$$

where k_{on} is the association rate constant. If we combine Equations 1 and 2, we find:

$$A_t = A_0 + (A_\infty - A_0) \cdot \frac{C_0 \cdot k_{on} \cdot t}{1 + C_0 \cdot k_{on} \cdot t}. \quad \mathbf{3}$$

Dissociation rate constants are not considered in these equations because they are negligible for the conditions and sequences studied. As discussed below, all solution-phase hybridizations reach 100% completion. The rate constant, k_{on}, can be obtained by calculation of C_t and linear fitting (Equation 2) or by nonlinear fits to the raw experimental data (Equation 3). For data which follow a two-state model, values of k_{on} obtained by either of these two fitting methods agree within 10% error.

Surface studies

Surface fabrication. The self-assembled DNA monolayers employed in all surface studies were fabricated according to a protocol developed previously in our laboratory (18). Briefly, the flat face of an SF-14 hemi-cylindrical prism was coated with ~1 nm chromium and ~50 nm gold after being cleaned with piranha solution (H_2SO_4:H_2O_2 = 7:3) for 10 min, rinsed with copious amounts of distilled water and dried under nitrogen. Thiolated DNA probe molecules were deprotected and used immediately. To obtain the probe densities used in these studies (4.5–6.8 × 10^{12} molecules/cm^2), a solution of 0.5 μM probe in 1 M KH_2PO_4 was injected into an all-Teflon flow cell sealed to the prism via o-ring and reacted for 4–5 h. This injection was followed by ~50°C hot water rinse to remove non-specifically bound DNA probe molecules from the surface. The surface was then back-filled by exposure to 0.5 mM mercaptohexanol in 1 M KH_2PO_4 for 5–6 h and rinsed with hot water again. After surface fabrication was complete, the surface was treated with 0.4% SDS (by weight in water) for 5 min and rinsed with distilled water.

All hybridization data presented in this study were obtained on surfaces with similar probe density (4.5–6.8 × 10^{12} molecules/cm^2). Because sequence content and secondary structure can affect the DNA probe coverage resulting from self assembly (19,20), the surface exposure time to both thiolated DNA probe and mercaptohexanol solutions was tuned in order to obtain probe densities in a narrow range.

Hybridization and regeneration of the DNA probe surface

Surface hybridization experiments were performed under the same ionic strength conditions used in the solution-phase studies at room temperature (~20°C). The probe surface was exposed to 1 μM ssDNA target strand in NaCl/TE buffer until equilibrium was attained. A control experiment, using non-complementary target, confirmed the absence of non-specific adsorption for each probe surface (data not shown). After hybridization, the probe surface (P_0, P_3 or P_4) was regenerated with 0.4% SDS and re-hybridized in various buffer solutions. We observed excellent reproducibility of hybridization kinetics and thermodynamics on the same surface, indicating the stability of probe films during experiments. Each probe surface could be SDS regenerated and re-hybridized >10 times.

SPR measurements

All surface DNA hybridization kinetic measurements were carried out via SPR spectroscopy. Detailed explanation of SPR theory, our experimental setup and data analysis methods have been given in earlier works (18,21,22). Briefly, we use a home-built SPR angle-scanning instrument to measure *in situ* reflectance from a gold-coated hemi-cylindrical prism at 632.8 nm. By fitting the obtained reflectivity profiles to a five-phase Fresnel optical model, we can obtain molecular surface coverage information. For the DNA submonolayers used in this study, probe and target coverages were determined by fixing the dielectric constant of the layer (ε_{layer}) at a value of 2.0 (19). Angularly dependent light scattering and ellipsometry studies have reported differences in ε_{layer} of 0.06–0.2 for ssDNA and dsDNA films (23,24). Our assumption of a single value of ε_{layer} for all probes with varying degrees of secondary structure, therefore, can cause at most 3% error in our coverage calculations. The refractive index increment (dn/dc) values for each individual strand employed in these studies were determined based on previous refractometer measurements of individual nucleotides and used to calculate surface coverage (19). It was assumed that the dn/dc value for dG, although not measured, was similar to that of dA. Hybridization efficiencies were determined by taking the ratio of calculated target coverage to the immobilized probe coverage.

Analysis of surface kinetics

Observed hybridization rate constants were obtained by fitting hybridization efficiency data to the first-order Langmuir equation:

$$\Gamma(t) = \Gamma_{max}[1 - \exp(-(k_{eff} \cdot C \cdot t))], \quad \mathbf{4}$$

where Γ_{max} is the maximal hybridization efficiency, k_{eff} is the effective rate constant for surface hybridization, and C is the target concentration (1 μM in this study). This equation assumes a homogeneous surface upon which all accessible binding sites are identical. In this work, dissociation rate constants are negligible (no target dissociation is observed during post-hybridization buffer rinse experiments) and therefore only one variable (k_{eff}) is considered in the fitting analysis for surface kinetic data. If the negligibly small dissociation rate constant was included as a second variable, then the resulting k_{eff} value obtained from fitting analysis would remain unchanged, although it would have a larger error.

RESULTS AND DISCUSSION

Secondary structure

In order to study the effects of ssDNA secondary structure on duplex formation, four sets of sequences were selected: P_0T_0, P_3T_3, P_4T_4 and P_4T_3 (Table 1). Each pair has a similar thermodynamic duplex stability but the number of base pairs involved in the individual ssDNA folded secondary structures varies. Duplex stability for each pair of sequences was confirmed by thermal melting experiments; all dsDNA pairs were found to have similar melting temperatures falling in a narrow range (ΔT_m < 2°C) (Supplementary Figure S2). This result rules out any stability effects on solution-phase

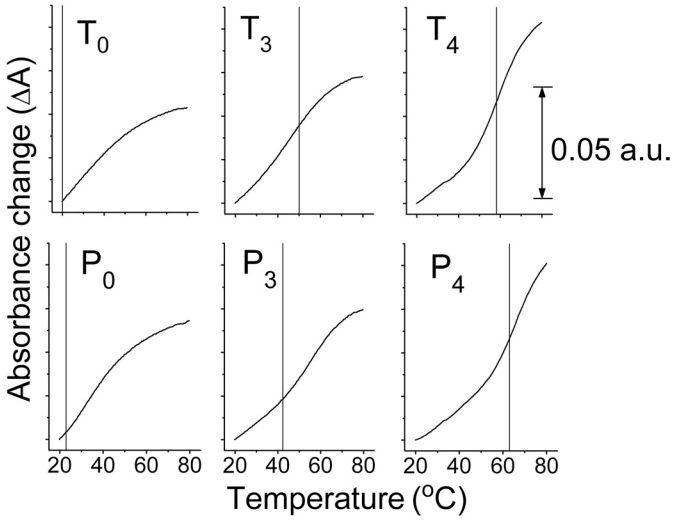

Figure 1. Thermal melting of ssDNA sequences monitored by UV absorbance spectroscopy. Sequences are listed in Table 1. Melting curves shown were collected at a ramp rate of 0.5°C/min for 2 μM ssDNA in 1 M NaCl/TE. Lines indicate the T_ms predicted by mFold for each sequence under these conditions.

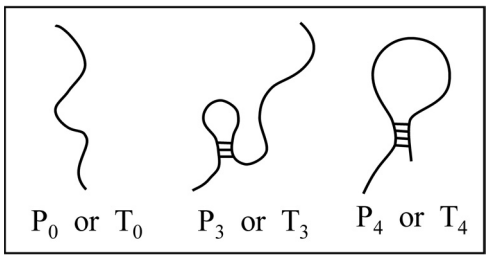

Scheme 1. Depiction of the forms for the sequences, illustrating lowest energy structures as predicted by mFold under conditions of 2 μM strand concentration and 1 M ionic strength. Structures contain no loops, a 5 base loop with 3 bp in the stem, and a 10 base loop with 4 bp in the stem, respectively, from left to right.

and surface hybridization kinetics measured in this study, particularly for the P_4T_3 duplex, which contains a 2 bp terminal mismatch. The terminal mismatch apparently has almost no effect on the thermodynamic duplex stability.

The secondary structure of each individual ssDNA sequence was qualitatively observed by thermal melting experiments (Figure 1). Only results in 1 M NaCl/TE are displayed, but the single strands behave similarly at all other ionic strengths studied (0.1 and 0.5 M, data not shown), exhibiting identical trends in absorbance change and melting profile. In general, as single-strand secondary structure increases, the absorbance change upon melting increases and the curve acquires a more sigmoidal shape. This shape appears as a result of the two states emerging in the strand at low and high temperatures: folded and unfolded, respectively. The magnitude of the absorbance change increases as both the number of base pairs unfolding and the hypochromicity of the strand increases.

The absorbance change that occurs over the temperature range measured for the P_0 and T_0 strands (left panel in Figure 1) is the result of base stacking. As the temperature increases, bases un-stack and the overall strand extinction coefficient increases. No sigmoidal shape is evident in these melting curves, indicating the absence of a folded state at low temperatures. The melting temperatures (T_ms) predicted by mFold for these strands under our solution conditions (denoted by the lines in Figure 1) also support a lack of secondary structure in these strands; the T_ms are at or below 20°C, indicating unfolded, random conformations for both P_0 and T_0.

Other strand melting temperatures predicted by mFold agree qualitatively well with our experimental data. The vertical lines in Figure 1 occur near the inflection points of the sigmoidal datasets obtained for P_3, T_3, P_4 and T_4. Scheme 1 displays the general lowest energy structures predicted by mFold for these strands. Sequences P_4 and T_4 are capable of forming similar 'hairpins' having 4 bp in the stem, 10 bp in the loop and a 6 bp tail. These structures are very stable, having predicted ΔG°_{20} values of −5.3 and −4.6 kcal/mol for P_4 and T_4, respectively. Similarly, sequences P_3 and T_3 are capable of forming 'hairpins' with 3 bp in the stem, 5 bp in the loop and two tails containing 4 and 10 bp. These structures are slightly less stable, having predicted ΔG°_{20} values of −3.1 and −3.8 kcal/mol for P_3 and T_3, respectively.

Although sequences containing intramolecular hairpin structure, such as P_4 and T_4, could form intermolecular dimers (P_4P_4 and T_4T_4), for our experimental conditions (Figure 1), this is not the case. Concentration-dependent thermal melting studies of ssDNA and van't Hoff analysis (Supplementary Figure S3) indicate that 90% of P_4 strands and 100% of T_4 strands exist as hairpins, rather than dimers at 20°C and 1 μM ssDNA. Therefore, we confine our discussion in this work to hairpin secondary structure.

Solution-phase kinetic measurements

We find that the presence of secondary structure in the individual single DNA strands slows the process of DNA hybridization profoundly. Figure 2 displays the solution-phase kinetics of duplex formation as monitored by UV absorbance spectroscopy and plotted in two different formats. A clear trend in the rate of absorbance change associated with hybridization is observed: $P_0T_0 > P_3T_3 > P_4T_3 > P_4T_4$. Duplexes P_0T_0, P_3T_3 and P_4T_3 form completely within 5 min, while the duplex having the most secondary structure in its single strands, P_4T_4, requires 1 h for formation. Although the kinetic data displayed in Figure 2 were measured in 0.5 M NaCl/TE, the same trend is observed for all other ionic strength buffers studied: 1 and 0.1 M NaCl/TE (Supplementary Figure S4).

Complete hybridization (100% efficiency) for all sequences was confirmed by thermally denaturing the duplexes immediately following single strand mixing and kinetic measurements. The same equilibrium absorbance value was re-established after slow strand annealing as was attained at 'infinite time' after room temperature mixing. For the hybridization of all sequences, the raw absorbance changes measured at room temperature scale well with the net number of base pairs formed during hybridization. For example, an absorbance change (ΔA) of 0.079 occurs during formation of the P_0T_0 duplex, which corresponds to the formation of 25 bp. However, the P_4T_4 individual single strands contain

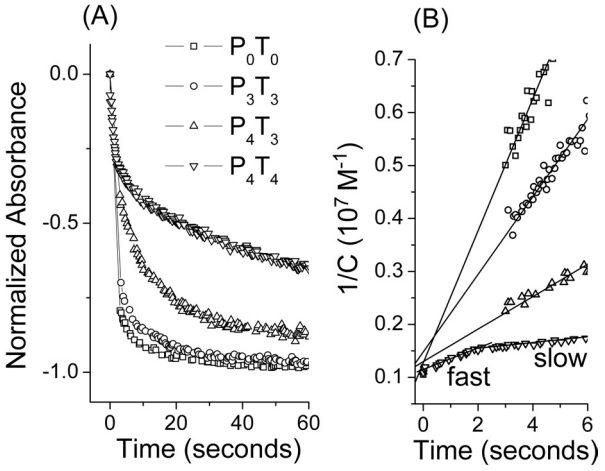

Figure 2. . Kinetics of DNA hybridization in solution. [Probe] = [Target] = 1 μM, T = 20°C, and [NaCl] = 0.5 M. (**A**) Normalized absorbance change upon injection or hand mixing of single strands as a function of time. The raw values of ΔA at 'infinite time' or equilibrium are 0.079, 0.063, 0.049 and 0.053 for P_0T_0, P_3T_3, P_4T_3 and P_4T_4, respectively. These values generally scale with the net number of Watson–Crick base pairs formed during hybridization (for details see text). (**B**) Linearized absorbance data plotted as inverse concentration versus time. Solid lines are fits to the data and the slopes correspond to the second-order hybridization rate constant for each set of sequences. Mixing of P_0T_0, P_3T_3 and P_4T_3 was done by hand pipetting, while P_4T_4 was carried out by syringe injection.

a total of eight pre-formed base pairs when mixed. As a result, a smaller ΔA of 0.053 is observed upon strand mixing that corresponds to the formation of an additional 17 bp during complete hybridization. This change in absorbance agrees closely with the theoretical value of 0.054 predicted from the P_0T_0 results for a net formation of 17 bp.

In order to obtain quantitative kinetic information about the effects of secondary structure on DNA hybridization, we fit the data in Figure 2A and B to Equations 3 and 2, respectively. Interestingly, the data for duplexes P_0T_0, P_3T_3 and P_4T_3, can be fit with a two-state model, whereas the P_4T_4 hybridization data cannot. Indeed, P_4T_4 (Figure 2B) requires two lines with different slopes to describe the duplex formation process. A simple two-state model is not appropriate for describing the hybridization of individual strands containing very stable intramolecular secondary structure, such as P_4T_4.

Rather, we propose that the two kinetic regimes measured for P_4T_4 can be explained by nucleation and zippering. According to Scheme 1, both P_4 and T_4 exist as hairpins, each with a 6 bp tail. The fast kinetic regime shown in Figure 2B may be the result of these tails nucleating or of their loops 'kissing', forming a partially hybridized species. The slow kinetic regime could then be caused by zippering of the remaining base pairs. This step is rate limiting because of the competition between intramolecular and intermolecular base pair formation. A slow displacement of the intramolecular base pairs in the hairpin stem must occur as the intermolecular base pairs are formed. Full-strand displacement of short oligomers has been measured by gel shift assay and shown to require hours for completion (25). Fluorescence correlation spectroscopy studies have also shown that spontaneous hairpin folding and unfolding in solution occurs in microseconds (26,27), indicating that our hybridization reactions are not limited by such a dissociative mechanistic step or pathway. In addition, the closed forms of the P_4 and T_4 strands are most likely favored under the room temperature, high-salt (>25 mM) conditions of our studies (28).

Table 2. Association DNA hybridization rate constants determined from solution-phase and surface measurements in 0.5 M NaCl/TE

Sequence	k (10^5 M^{-1} s^{-1}) Solution	Surface
P_0T_0	12.0 ± 0.6	0.57 ± 0.04
P_3T_3	7.2 ± 0.3	0.24 ± 0.01
P_4T_3	3.0 ± 0.1	0.083 ± 0.003
P_4T_4	2.0 ± 0.1 (fast) 0.48 ± 0.01 (slow)	0.032 ± 0.001

Errors represent uncertainty in fitting single trial data to either Equation 2 (solution) or Equation 4 (surface); trial-to-trial errors are, at most, 7%.

Table 2 lists the association rate constants determined from solution-phase and surface measurements in 0.5 M NaCl/TE. The surface association rate constants are discussed in the next section. For all four duplexes listed in the left panel of Table 2, the solution rate constants were obtained from fits to Equation 2, assuming that the entire absorbance change observed over time is caused by the formation of a full duplex (25 bp). For P_4T_4, a single rate constant cannot account for the data and values are provided for both the fast and slow kinetic regime.

For the fast kinetic regime, if we assume that the observed absorbance change is caused by the formation of a six nucleation base pair tail rather than all 25 bp and calculate a rate constant based on Equation 2, we find $k_{on} = (12.5 \pm 0.4) \times 10^5$ M^{-1} s^{-1}. This value agrees with the association rate constant measured for the probe–target pair devoid of any secondary structure, P_0T_0. This supports our proposed mechanism of tail nucleation followed by strand displacement for P_4T_4 during the fast kinetic regime.

Surface kinetic measurements

The trend observed for hybridization rates in solution is also observed for target hybridization to surface-immobilized probe ssDNA at all ionic strengths studied. Surface hybridization data measured in 0.5 M NaCl/TE are plotted in Figure 3 (for other ionic strength data see Supplementary Figure S5). Duplex P_0T_0 forms the fastest, reaching equilibrium in 3 min, while P_4T_4 is undoubtedly the slowest, requiring hours for complete duplex formation. This kinetic trend in rate constants, $P_0T_0 > P_3T_3 > P_4T_3 > P_4T_4$, is clearly displayed by the normalized data presented in the inset of Figure 3. Given the results in solution, this trend is reasonable. However, there are results in the literature that suggest probe and target secondary structure do not affect surface hybridization rate (16).

We do, nevertheless, find significant differences between solution and surface hybridization kinetics, discussed below, and hybridization thermodynamics. Solution-phase hybridizations are able to achieve 100% hybridization efficiency or completion given equal molar quantities of probe and target, while surface hybridizations reach only 15–25%

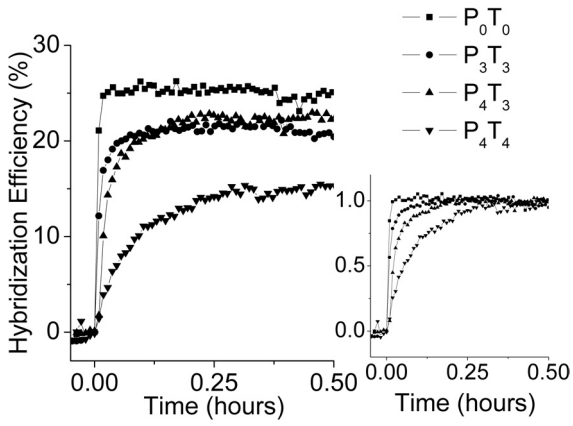

Figure 3. Surface hybridization kinetics. Hybridizations are monitored for many hours, but only shown on a 30 min time-scale here. Hybridization of duplexes P_0T_0 and P_3T_3 is very fast, while hybridization of P_4T_4 is very slow. Duplex P_4T_4 reaches 20% hybridization efficiency, but only after overnight target exposure. For all hybridizations, [Target] = 1 μM, T = 20°C, and [NaCl] = 0.5 M. Exposure of each probe surface to control target strands yields no significant binding (data not shown). Probe densities are 4.5×10^{12}, 6.8×10^{12} and 5.7×10^{12} molecules/cm^2 for P_0, P_3 and P_4 probe surfaces, respectively. (Inset) Hybridizations normalized at 30 min for comparison of kinetic rates.

efficiency under conditions of target saturation. This is most probably a consequence of the steric and electrostatic hindrance caused by the confinement of ssDNA on the surface; a large percentage of probe is not target accessible. Duplexes P_0T_0, P_3T_3 and P_4T_3 also achieve the same efficiency within our ~7% coverage calculation error associated with assumption of an isotropic refractive index for DNA (19) and our surface-to-surface variation of 8–9%. Duplex P_4T_4, however, only attains 15% efficiency after 30 min. Secondary structure clearly imposes some additional thermodynamic barrier to hybridization, which is particularly dominant at low ionic strengths (Supplementary Figure S5C).

Secondary structure effects on surface hybridization kinetics are quantitated by fitting the measured data to a traditional Langmuir model, Equation 4. Effective association rate constants, determined by fitting the first 30 minutes of hybridization data, are listed in the right panel of Table 2. Values obtained are independent of probe density, as we limited the surfaces studied to a narrow density range, 4.5–6.8 × 1012 molecules/cm^2. We have shown previously that kinetics can vary over wide ranges of probe density, but remain virtually unaffected by densities in narrow or similar regimes (29).

As secondary structure increases, the uncertainty (error) obtained from fitting the data to a Langmuir model beyond 30 min increases. For P_0T_0, the error associated with the hybridization rate constant is 5–7% for all time scales fit, whereas the error obtained from fitting P_4T_3 hybridization is 30% on long time scales (2 h). The Langmuir model, however, completely fails to fit the P_4T_4 data beyond 30 min; the hybridization process is very slow and does not follow a simple two-state physical mechanism (for data fits see Supplementary Figure S5). Another model, such as that used to describe hybridization to structured probes containing G-quartets (29,30), could be applied to the P_4T_4 system. Additional fitting parameters needed to describe the rates of folding and unfolding of the probe may add uncertainty. This model was found to predict faster hybridization rates for probes containing secondary structure compared to 'random' sequences, in contrast to our observed trend. Clearly better models are needed to describe the surface data, perhaps including site interactions.

Comparison of surface and solution-phase results

DNA hybridization has been studied extensively in bulk solution and on a variety of solid supports using a number of different experimental techniques and conditions. Because of differences in ionic strength, pH, strand sequence and concentration, temperature, and buffer additives, it is often difficult to compare measurements of hybridization in solution and on the surface. It is known that the solid support affects DNA hybridization on surfaces (31), but few studies have attempted to systematically quantify this effect. The lack of *in situ* experimental comparative data makes it difficult to predict the performance of surface biosensors from calculated or observed solution-phase behavior.

Here, we have systematically studied the kinetics of DNA hybridization in both surface and solution-phase environments. Of course, our comparison is based on measurements from two techniques monitoring different events: solution-phase UV absorbance measurements probing base pair formation and SPR measurements indirectly probing 'target recognition'. Recent work (32) suggests that surface analytical methods such as QCM and SPR do not detect complete duplex hybridization, but instead, detect duplex nucleation or 'initial target recognition'. Their voltammetry studies indicate that complete zippering of the duplex on the surface requires hours instead of the mere minutes measured under the same conditions by QCM. Nevertheless, it has long been accepted that the rate-limiting step in solution-phase DNA hybridization of short strands such as those studied here is nucleation (33). As a result, solution-phase hybridization rates reflecting nucleation or some combination of nucleation and displacement, are comparable to SPR measurements.

For each of our sequence pairs, the associative kinetics of surface DNA hybridization are suppressed by a factor of 20- to 40-fold compared to solution-phase hybridization (Table 2). This result compares favorably with the 5- to 10-fold suppression in hybridization rates of 22mers observed with FRET on microparticles (34). In general, surface suppression is likely caused by steric and electrostatic hindrance present in the DNA probe film as well as conformational restriction of the surface-tethered strands. As a result, the surface kinetic suppression factor we have determined for thiolated DNA immobilized on gold will likely be affected by changes in probe attachment and density. Based on previous studies (1,32,35), we predict that DNA hybridization rates will increase at lower probe densities and for probe films containing spacers, but it is not clear at this time whether any measurable, biosensor-relevant condition exists for which solution and surface hybridization rates agree.

We have also observed that secondary structure present in the individual DNA single strands suppresses the DNA hybridization kinetics in both the surface and solution-phase environments. Figure 4 displays this suppression with a plot of measured solution and surface associative rate constants versus the degree of secondary structure in the

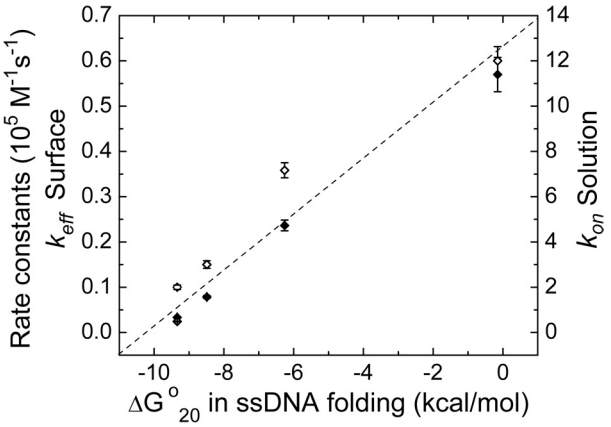

Figure 4. Comparison of k_{eff} (left axis, closed diamond) and k_{on} (right axis, open diamond) versus ΔG°_{20} of ssDNA folding in bulk solution and on the surface, respectively. Plotted values of ΔG°_{20} for each single strand involved in the duplex were calculated by mFold and combined. Calculations with mFold were carried out under the same conditions employed in our experiments. The dotted line is a guide to the eye.

duplex-forming probe and target strands (combined ΔG°_{20} values calculated from mFold for each strand). The measured hybridization rate constants in solution and on the surface have a similar linear relationship with the stability of secondary structure when scaled. A previous solution–surface comparison (16) also reported a secondary structure trend in hybridization kinetics for a series of designed hairpins, but only in solution. No dependence on secondary structure was observed for fluorescence-based surface studies with identical sequences. This may have been caused by excessive probe loss during the *ex situ* rinsing of the probe-modified beads employed or by probe-surface fluorophore quenching.

The data in Figure 4 suggest that adding three intramolecular base pairs to the probe and target strands involved in duplex formation (~ -6 kcal/mol combined stability) causes a 2-fold decrease in hybridization rate both in solution and on the surface. This exact factor could change slightly depending on the sequence composition, length or structure selected in the probe design process. In general, adding a G·C rather than an A·T base pair to the stem causes greater hairpin stability and could decrease the hybridization kinetics more profoundly. The size and rigidity of the hairpin loop have been shown to affect thermodynamic stability (26,36,37) and could also affect duplex formation rates. In addition, the length of hairpin 'tails', which can be sites for duplex nucleation according to our proposed hybridization mechanism, may be important to kinetic rates. Nevertheless, we have provided a general relationship between the stability of secondary structure in the individual strands involved and the resultant hybridization kinetics. Although they are suppressed, the DNA hybridization rates observed on the surface mirror those measured in solution. This finding may have implications for the selection of experimental conditions and probe sequences used in conjunction with surface-based biosensors.

CONCLUSIONS

We have shown that probe and target secondary structure affect the DNA hybridization kinetics both in solution and on the surface. Although the planar gold surface and probe layer environment suppress the measured rates 20- to 40-fold, the effects of secondary structure are similar in solution and surface environments. We have provided a general correlation between probe and target intramolecular structures predicted by computational algorithms such as mFold and the hybridization kinetics observed for these species. These results may be applied to ongoing work in our lab on aptamer-based biosensors and, more generally, to probe design for other DNA-based sensors.

SUPPLEMENTARY DATA

Supplementary Data are available at NAR online.

ACKNOWLEDGEMENTS

We acknowledge fruitful discussions with Lucian Postelnicu at Boston University. This work is supported by the National Cancer Institute of the NIH (CA 89562) and the National Science Foundation (DBI-0096731). This work was partially supported by the Army Research Laboratory (Cooperative Agreement DAAD19-00-2-0004) and resources at the Boston University Photonics Center. Funding to pay the Open Access publication charges for this article was provided by the NIH and the Department of Chemistry, Boston University.

Conflict of interest statement. None declared.

REFERENCES

1. Okahata,Y., Kawase,M., Niikura,K., Ohtake,F., Furusawa,H. and Ebara,Y. (1998) Kinetic measurements of DNA hybridisation an oligonucleotide-immobilized 27-MHz quartz crystal microbalance. *Anal. Chem*., **70**, 1288–1296.
2. Xu,J. and Craig,S.L. (2005) Thermodynamics of DNA hybridization on gold nanoparticles. *J. Am. Chem. Soc*., **127**, 13227–13231.
3. Wetmur,J.G. and Davidson,N. (1968) Kinetics of renaturation of DNA. *J. Mol. Biol*., **31**, 349–370.
4. Morrison,L.E. and Stols,L.M. (1993) Sensitive fluorescence-based thermodynamic and kinetic measurements of DNA hybridization in solution. *Biochemistry*, **32**, 3095–3104.
5. SantaLucia,J. (1998) A unified view of polymer, dumbbell, and oligonucleotide DNA nearest-neighbor thermodynamics. *Proc. Natl Acad. Sci. USA*, **95**, 1460–1465.
6. Peyret,N., Seneviratne,P.A., Allawi,H.T. and SantaLucia,J. (1999) Nearest-neighbor thermodynamics and NMR of DNA sequences with internal A·A, C·C, G·G and T·T mismatches. *Biochemistry*, **38**, 3468–3477.
7. Peyret,N. (2000) Prediction of nucleic acid hybridization: parameters and algorithms. PhD Dissertation. Wayne State University, Detroit, MI.
8. Zuker,M. (2003) Mfold web server for nucleic acid folding and hybridization prediction. *Nucleic Acids Res*., **31**, 3406–3415.
9. Holbrook,J.A., Capp,M.W., Saecker,R.M. and Record,M.T. (1999) Enthalpy and heat capacity changes for formation of an oligomeric DNA duplex: interpretation in terms of coupled processes of formation and association of single-stranded helices. *Biochemistry*, **38**, 8409–8422.
10. Studier,F.W. (1969) Effects of conformation of single-stranded DNA on renaturation and aggregation. *J. Mol. Biol*., **41**, 199–209.
11. Lima,W.F., Monia,B.P., Ecker,D.J. and Freier,S.M. (1992) Implication of RNA structure on antisense oligonucleotide hybridization kinetics. *Biochemistry*, **31**, 12055–12061.
12. Schwille,P., Oehlenschlager,F. and Walter,N.G. (1996) Quantitative hybridization kinetics of DNA probes to RNA in solution followed by

diffusional fluorescence correlation analysis. *Biochemistry*, **35**, 10182–10193.
13. Vesnaver,G. and Breslauer,K.J. (1991) The contribution of DNA single-stranded order to the thermodynamics of duplex formation. *Proc. Natl Acad. Sci. USA*, **88**, 3569–3573.
14. Kushon,S.A., Jordan,J.P., Seifert,J.L., Nielsen,H., Nielsen,P.E. and Armitage,B.A. (2001) Effect of secondary structure on the thermodynamics and kinetics of PNA hybridization to DNA hairpins. *J. Am. Chem. Soc.*, **123**, 10805–10813.
15. Bonnet,G., Tyagi,S., Libchaber,A. and Kramer,F.R. (1999) Thermodynamic basis of the enhanced specificity of structured DNA probes. *Proc. Natl Acad. Sci. USA*, **96**, 6171–6176.
16. Sekar,M.M.A., Bloch,W. and St John,P.M. (2005) Comparative study of sequence-dependent hybridization kinetics in solution and on microspheres. *Nucleic Acids Res.*, **33**, 366–375.
17. Chien,F.C., Liu,J.S., Su,H.J., Kao,L.A., Chiou,C.F., Chen,W.Y. and Chen,S.J. (2004) An investigation into the influence of secondary structures on DNA hybridization using surface plasmon resonance biosensing. *Chem. Phys. Lett.*, **397**, 429–434.
18. Peterlinz,K.A., Georgiadis,R.M., Herne,T.M. and Tarlov,M.J. (1997) Observation of hybridization and dehybridization of thiol-tethered DNA using two-color surface plasmon resonance spectroscopy. *J. Am. Chem. Soc.*, **119**, 3401–3402.
19. Wolf,L.K., Gao,Y. and Georgiadis,R.M. (2004) Sequence-dependent DNA immobilization: specific versus nonspecific contributions. *Langmuir*, **20**, 3357–3361.
20. Steichen,M. and Buess-Herman,C. (2005) Electrochemical detection of the immobilization and hybridization of unlabeled linear and hairpin DNA on gold. *Electrochem. Commun.*, **7**, 416–420.
21. Peterlinz,K.A. and Georgiadis,R.M. (1996) *In situ* kinetics of self-assembly by surface plasmon resonance spectroscopy. *Langmuir*, **12**, 4731–4740.
22. Georgiadis,R.M., Peterlinz,K.A. and Peterson,A.W. (2000) Quantitative measurements and modeling of kinetics in nucleic acid monolayer films using SPR spectroscopy. *J. Am. Chem. Soc.*, **122**, 3166–3173.
23. Elhadj,S., Singh,G. and Saraf,R.F. (2004) Optical properties of an immobilized DNA monolayer from 255 to 700 nm. *Langmuir*, **20**, 5539–5543.
24. Henke,L., Piunno,P.A.E., Nagy,N., Wust,C.C. and Krull,U.J. (2001) Rapid and simple technique for the determination of the refractive index of ultra-thin organic films on planar transparent substrates using forward light scatter. *Anal. Chim. Acta*, **433**, 31–45.
25. Reynaldo,L.P., Vologodskii,A.V., Neri,B.P. and Lyamichev,V.I. (2000) The kinetics of oligonucleotide replacements. *J. Mol. Biol.*, **297**, 511–520.
26. Jung,J.M. and Van Orden,A. (2005) Folding and unfolding kinetics of DNA hairpins in flowing solution by multiparameter fluorescence correlation spectroscopy. *J. Phys. Chem. B*, **109**, 3648–3657.
27. Bonnet,G., Krichevsky,O. and Libchaber,A. (1998) Kinetics of conformational fluctuations in DNA hairpin-loops. *Proc. Natl Acad. Sci. USA*, **95**, 8602–8606.
28. Jung,J.M. and Van Orden,A. (2006) A three-state mechanism for DNA hairpin folding characterized by multiparameter fluorescence fluctuation spectroscopy. *J. Am. Chem. Soc.*, **128**, 1240–1249.
29. Zhao,Y., Kan,Z.Y., Zeng,Z.X., Hao,Y.H., Chen,H. and Tan,Z. (2004) Determining the folding and unfolding rate constants of nucleic acids by biosensor. Application to telomere G-quadruplex. *J. Am. Chem. Soc.*, **126**, 13255–13264.
30. Halder,K. and Chowdhury,S. (2005) Kinetic resolution of bimolecular hybridization versus intramolecular folding in nucleic acids by surface plasmon resonance: application to G-quadruplex/duplex competition in human c-myc promoter. *Nucleic Acids Res.*, **33**, 4466–4474.
31. Levicky,R. and Horgan,A. (2005) Physicochemical perspectives on DNA microarray and biosensor technologies. *Trends Biotechnol.*, **23**, 143–149.
32. Wong,E.L.S., Chow,E. and Gooding,J.J. (2005) DNA recognition interfaces: the influence of interfacial design on the efficiency and kinetics of hybridization. *Langmuir*, **21**, 6957–6965.
33. Tinoco,I., Crothers,D.M. and Bloomfield,V.A. (2000) *Nucleic Acids: Structure, Properties and Functions*. Chapter 8. University Science Books, Sausalito, CA.
34. Henry,M.R., Stevens,P.W., Sun,J. and Kelso,D.M. (1999) Real-time measurements of DNA hybridization on microparticles with fluorescence resonance energy transfer. *Anal. Biochem.*, **276**, 204–214.
35. Peterson,A.W., Heaton,R.J. and Georgiadis,R.M. (2001) The effect of surface probe density on DNA hybridization. *Nucleic Acids Res.*, **29**, 5163–5168.
36. Du,H., Disney,M.D., Miller,B.L. and Krauss,T.D. (2003) Hybridization-based unquenching of DNA hairpins on Au surfaces: prototypical 'molecular beacon' biosensors. *J. Am. Chem. Soc.*, **125**, 4012–4013.
37. Du,H., Strohsahl,C.M., Camera,J., Miller,B.L. and Krauss,T.D. (2005) Sensitivity and specificity of metal surface-immobilized 'molecular beacon' biosensors. *J. Am. Chem. Soc.*, **127**, 7932–7940.